HHS Public Access

Author manuscript

Dev Cell. Author manuscript; available in PMC 2018 February 27.

Published in final edited form as:

Dev Cell. 2017 February 27; 40(4): 367–380.e7. doi:10.1016/j.devcel.2017.01.014.

A Hdac1/Rpd3-poised circuit balances continual self-renewal and rapid restriction of developmental potential during asymmetric stem cell division

Derek H. Janssens[1,2], **Danielle C. Hamm**[3], **Lucas Anhezini**[2], **Qi Xiao**[4,**], **Karsten H. Siller**[5], **Sarah E. Siegrist**[6], **Melissa M. Harrison**[3], and **Cheng-Yu Lee**[1,2,4,7,*]

[1]Cellular and Molecular Biology Graduate Program, University of Michigan Medical School, Ann Arbor, MI, 48109

[2]Life Sciences Institute, University of Michigan, Ann Arbor, MI, 48109

[3]Department of Biomolecular Chemistry, University of Wisconsin Madison, WI 53706

[4]Department of Cell and Developmental Biology, University of Michigan Medical School, Ann Arbor, MI, 48109

[5]Advanced Research Computing Services, University of Virginia, Charlottesville, VA 22904

[6]Department of Biology, University of Virginia, Charlottesville, VA 22904

[7]Division of Molecular Medicine and Genetics, Department of Internal Medicine, University of Michigan Medical School, Ann Arbor, MI, 48109

Summary

How the developmental potential of differentiating stem cell progeny becomes rapidly and stably restricted following asymmetric stem cell division is unclear. In the fly larval brain, *earmuff* (*erm*) uniquely functions to restrict the developmental potential of intermediate neural progenitors (INPs) generated by asymmetrically dividing neural stem cells (neuroblasts). Here we demonstrate that the histone deacetylase Hdac1/Rpd3 functions together with self-renewal transcriptional repressors to maintain the *erm* immature INP enhancer in an inactive but poised state in neuroblasts. Within two-hours of immature INP birth, down-regulation of repressor activities alleviates Rpd3-mediated repression on the *erm* enhancer, enabling acetylation of multiple histone proteins and activating Erm expression. Erm restricts the developmental potential in immature INPs by repressing genes encoding neuroblast transcriptional activators. We propose that poising the fast-activating enhancers of master regulators of differentiation through continual histone

*Corresponding Author and Lead Contact: leecheng@umich.edu.

**Current Address: Department of Biological Chemistry, University of California, Los Angeles, CA 90095

Author Contribution

D.J., D.H., L.A., Q.X., K.S. and S.S. conducted the experiments. D.J., D.H., M.H. and C.L. designed the experiments, and wrote the manuscript.

deacetylation in stem cells enables self-renewal and rapid restriction of developmental potential following asymmetric division.

Introduction

To produce the astounding number and diversity of cells that comprise our body, stem cells undergo countless rounds of asymmetric division to self-renew while simultaneously giving rise to more restricted cell types. To amplify the output of each division, stem cells generate intermediate progenitors that possess restricted developmental potential, and produce exclusively differentiated cell types (Paridaen and Huttner, 2014). If their developmental potential is not stably restrained, intermediate progenitors may become susceptible to oncogenic transformation (Alcantara Llaguno et al., 2015; Chen et al., 2010). Thus, the mechanisms that restrict the developmental potential of intermediate progenitors must be executed in an extremely efficient and robust manner to ensure normal development and tissue homeostasis.

In vertebrate stem cells, the cell type-specific enhancers of key developmental regulators are maintained in a poised chomatin state for subsequent activation in their differentiating progeny (Calo and Wysocka, 2013; Heinz et al., 2015; Zentner et al., 2011). These poised enhancers are enriched for mono- and di-methylated lysine 4 on histone H3 (H3K4me1/2), catalyzed by the Trithorax (Trx) family of proteins, and trimethylated lysine 27 on histone H3 (H3K27me3), catalyzed by Polycomb Repressive Complex 2 (PRC2). This model suggests that the trimethylation of H3K27 precludes CBP-catalyzed acetylation, and prevents premature activation of these poised enhancers in stem cells. Nonetheless, whether the conversion of H3K27me3 to H3K27ac indeed plays an instructive role in poised enhancer activation is unclear. In addition, whether this mechanism is kinetically feasible to trigger the expression of master regulators of differentiation in stem cell progeny remains untested.

The mechanisms that restrict the developmental potential of intermediate progenitors remain unknown partly due to lack of a well-defined window during which this process occurs in most stem cell lineages. A subset of neural stem cells (type II neuroblasts) in the fly larval brain undergo repeated asymmetric divisions to generate immature intermediate neural progenitors (INPs) that acquire restricted developmental potential through a process called maturation lasting 8-10 hours after their birth (Bello et al., 2008; Boone and Doe, 2008; Bowman et al., 2008; Janssens and Lee, 2014; Weng and Lee, 2011). Following maturation, INPs re-enter the cell cycle and undergo 5-6 rounds of asymmetric divisions to produce exclusively differentiating progeny (Bayraktar and Doe, 2013; Viktorin et al., 2011). Immature INPs can be unambiguously identified based on the proximity to their parental type II neuroblast and a well characterized set of molecular markers, providing an excellent genetic model for investigating how the developmental potential of intermediate progenitors is restricted *in vivo* (Figure 1A).

Restriction of the developmental potential in immature INPs occurs through a highly orchestrated mechanism. The tumor suppressor proteins Brain tumor (Brat) and Numb asymmetrically segregate into the newly born immature INP, and down-regulate the function

of self-renewal genes *klumpfuss* (*klu*), *deadpan* (*dpn*) and *Enhancer of split mγ* (*E(spl)mγ*) (Berger et al., 2012; Haenfler et al., 2012; Janssens et al., 2014; Komori et al., 2014b; Xiao et al., 2012). Down-regulation of self-renewal genes coincides with the onset of *earmuff* (*erm*) expression in immature INPs (Figure 1A). Once activated, Erm stably restricts the developmental potential of immature INPs because (1) *erm* null INPs spontaneously revert into supernumerary type II neuroblasts, and (2) mis-expression of *erm* triggers premature neuroblast differentiation (Janssens et al., 2014; Li et al., 2016; Weng et al., 2010). The molecular mechanisms by which Erm and its vertebrate homologs Fezf1 and Fezf2 regulate gene transcription are likely conserved (Janssens et al., 2014; Weng et al., 2010; Zhang et al., 2014). However, discrepancies between the reported DNA binding sequences of Erm and Fezf2 have hindered identification of the direct targets of this family of transcription factors (Chen et al., 2011; Koe et al., 2014). Elucidating a physiologically relevant Erm-binding sequence, and identifying Erm targets within the fly genome will significantly improve our understanding of the role of the Fezf family of transcription factors during neurogenesis.

In this study, we demonstrated that maintaining the cell type-specific enhancer of *erm* in a poised state in self-renewing type II neuroblasts enables rapid onset of Erm expression in immature INPs within two hours of their birth. Contrary to expectation, the *erm* immature INP enhancer requires the histone deacetylase Hdac1/Rpd3, but not PRC2, to remain inactive in type II neuroblasts despite displaying H3K27me3. We found that the transcriptional repressors Klu, Dpn and E(spl)mγ bind the *erm* immature INP enhancer in type II neuroblasts, and function together with Rpd3 to promote self-renewal by preventing premature *erm* activation. In parallel, the type II neuroblast-specific ETS1 transcriptional activator Pointed (PntP1) also binds this enhancer, and promotes its activation. Most surprisingly, we found that two histone acetyltransferases (HATs), Tip60 and HBO1, likely activate *erm* expression through acetylation of multiple histone proteins. These results strongly suggest that down-regulation of Klu, Dpn and E(spl)mγ in the immature INP alleviates Rpd3-mediated repression, permitting a rapid burst of histone acetylation on the *erm* immature INP enhancer to trigger Erm expression. Lastly, we identified and validated a functional Erm-binding sequence that is also recognized by Fezf1 and Fezf2 *in vitro*. We showed that Erm restricts the developmental potential in immature INPs by directly repressing the expression of *pntP1* and the O-isoform of *grainy head* (*grhO*), which encode neuroblast transcriptional activators. This work provides a new paradigm in which removal of self-renewal transcriptional repressors and repression by histone deacetylation, rather than addition of a transcriptional activator, triggers fast-activating poised gene expression in differentiating stem cell progeny. We propose this Rpd3-poised negative feedback circuit as a highly efficient and robust mechanism to balance continual self-renewal with rapid restriction of developmental potential across asymmetric stem cell division.

Results

erm is poised in type II neuroblasts for rapid activation in their immature INP progeny

To unravel the mechanisms that initiate restriction of the developmental potential in immature INPs, we examined the expression pattern of the *R9D-Gal4* drivers controlled by various *cis*-regulatory fragments from the *erm* locus (Pfeiffer et al., 2008). We found two

partially overlapping fragments, 9D10 and 9D11, that can individually drive reporter expression in immature INPs (data not presented). To facilitate rapid mapping and functional analysis of *Drosophila* enhancers, we created a series of VanGlow-GFP::Luciferase(nls) or VanGlow-mCherry::Renilla(nls) vectors (Supplementary Figures 1A-B). We confirmed that the overlapping region between the 9D10 and 9D11 fragments can activate reporter expression in immature INPs, and named this region the 9D11^{1} enhancer (Figure 1B; data not presented). In addition, the region of the 9D11 fragment that does not overlap with the 9D10 fragment also drives reporter expression in immature INPs, and we named this region the 9D11^{2} enhancer (Figure 1B; data not presented). We focused on the 9D11^{2} enhancer, and mapped it to a minimal 250-bp fragment (9D11$^{2\text{-}5}$) that becomes activated in a pattern reminiscent of endogenous Erm in immature INPs as revealed by the *9D11$^{2\text{-}5}$-GFP::Luc(nls)* transgene (referred to as *9D11$^{2\text{-}5}$-GFP* hereafter) (Figures 1B-C; Supplementary Figure 1). We conclude that the 9D11$^{2\text{-}5}$ enhancer contains key regulatory elements that confer the specificity of *erm* activation in immature INPs.

To estimate the kinetics of *erm* activation in the immature INP, we examined the timing of *9D11$^{2\text{-}5}$-GFP* activation following asymmetric neuroblast division by live-cell imaging. We marked all cells in the type II neuroblast lineage with a mCherry(nls), and found that 9D11$^{2\text{-}5}$-GFP becomes detectable in the immature INP less than two hours after neuroblast division (Figures 1D-E; Supplementary Movie 1). Thus, *erm* activation and the onset of restriction of the developmental potential in the immature INP occurs within two hours of its birth (Figure 1F).

This rapid activation of the 9D11$^{2\text{-}5}$ enhancer in immature INPs led us to hypothesize that *erm* is maintained in an inactive but poised state in type II neuroblasts. To test this hypothesis, we performed chromatin immunoprecipitation coupled with quantitative PCR analyses on the nuclear extract from either larval brains expressing a *UAS-aPKC^{caax}* transgene driven by *Ase*-Gal4, which contain thousands of supernumerary type I neurobasts, or *brat* null larval brains, which contain thousands of supernumerary type II neuroblasts (Haenfler et al., 2012; Komori et al., 2014a). To validate that these nuclear extracts provide reliable sources of the type I and type II neuroblast-enriched chromatin respectively, we first examined the relative enrichment of *pntP1* and *buttonhead* (*btd*), which are specifically expressed in type II neuroblasts (Komori et al., 2014a; Xiao et al., 2012; Xie et al., 2014; Zhu et al., 2011). In the type II neuroblast-enriched chromatin, the transcriptional start sites (TSS) of both genes were marked by high levels of H3K4me2 and H3K27ac that indicate active transcription, but in the type I neuroblast-enriched chromatin, the TSS of both genes were marked by high levels of H3K4me2 and H3K27me3 that indicate inactive transcription (Figures 1G-H). In addition, the TSS of *grhO*, which is expressed in all larval brain neuroblasts (Almeida and Bray, 2005), was marked by H3K4me2 and H3K27ac in both type I neuroblast-enriched and type II neuroblast-enriched chromatin (Figures 1G-H). Finally, we examined the TSS of two components of the Bithorax Complex, *Ultrabithorax* (*Ubx*) and *abdominal B* (*abd-B*), which are classic targets of PRC2 and Trx, but are not expressed in larval brain neuroblasts (Bello et al., 2007). In both type I and type II neuroblast-enriched chromatin, the TSS of *Ubx* and *abd-B* displayed high levels of H3K27me3 that correlate with inactive transcription (Figures 1G-H). Thus, the type I and type II neuroblast-enriched

nuclear extracts provide a reliable platform to examine the chromatin signature of genes in distinct larval brain neuroblast lineages.

We next examined the chromatin state of the *erm* locus in the type I and type II neuroblast-enriched nuclear extracts. The TSS of *erm* was enriched for H3K4me2 and H3K27me3 in both type I and type II neuroblast-enriched chromatin, suggesting *erm* is maintained in a poised state in both types of neuroblasts (Figures 1G-H). Furthermore, the $9D11^{2-5}$ enhancer in the *erm* locus ($9D11^{2-5}$(endo)) was enriched for H3K4me2 and H3K27me3 (Figure 1I). Thus, we conclude that maintaining the *erm* promoter and its immature INP enhancer in a poised state in self-renewing type II neuroblasts likely contributes to rapid *erm* activation in immature INPs following asymmetric neuroblast division.

Rpd3 but not PRC2 maintains *erm* inactive in type II neuroblasts by poising its immature INP enhancer

Because activation of *$9D11^{2-5}$-GFP* coincides with the onset of endogenous Erm expression in immature INPs (Figure 1C), we used the $9D11^{2-5}$ enhancer in this transgene ($9D11^{2-5}$(tran)) as a tool to investigate regulation of the poised *erm* enhancer. We first examined if the $9D11^{2-5}$(tran) enhancer is enriched for H3K4me2 and H3K27me3 in the type II neuroblast-enriched chromatin, similar to the $9D11^{2-5}$(endo) enhancer. Surprisingly, the $9D11^{2-5}$(tran) enhancer displayed high levels of H3K4me2 but not H3K27me3 in the type II neuroblast-enriched chromatin, despite remaining inactive in type II neuroblasts (Figures 1C and 1I). This unexpected result prompted us to test if the $9D11^{2-5}$(tran) enhancer is indeed poised in type II neuroblasts. Trx specifically catalyzes the formation of H3K4me1/2, and contributes to the maintenance of poised enhancers (Rickels et al., 2016). We found that knocking down *trx* function significantly reduced *$9D11^{2-5}$-GFP* activity (Figure 2A). Thus, we conclude that the $9D11^{2-5}$(tran) enhancer is indeed maintained in a poised state in type II neuroblasts.

Our finding that H3K27me3 is absent from the $9D11^{2-5}$(tran) enhancer suggests PRC2 may not be required to prevent premature activation of the *erm* immature INP enhancer in type II neuroblasts. *Enhancer of zeste* (*E(z)*) and *Suppressor of zeste 12* (*Su(z)12*) encode two core components of PRC2, and are essential for catalyzing the repressive H3K27me3 histone modification (Blackledge et al., 2015). We found that by 72 hours after clone induction, *Su(z)12* null type II neuroblasts displayed undetectable H3K27me3, and that by 96 hours after clone induction, neuroblasts in the majority of *E(z)* null clones were also H3K27me3 negative (Figures 2B-C and 2H; data not presented). We next examined the expression of *Ubx* and *abd-B*. Interestingly, we found that while Ubx and Abd-B were both undetectable in wild-type type II neuroblasts, only Abd-B became ectopically activated in *Su(z)12* and *E(z)* null type II neuroblasts, indicating that these genes are differentially regulated in type II neuroblasts (Figures 2D-E and 2H; Supplementary Figures 2A-B; data not presented). In *Su(z)12* and *E(z)* null clones, Erm expression was never detected in type II neuroblasts, and became significantly reduced in immature INPs instead (Figures 2F-I; data not presented). These data indicate that PRC2 does not prevent premature Erm expression, and that an alternative mechanism exists to maintain *erm* inactive in type II neuroblasts by poising its immature INP enhancer.

Because both the 9D11$^{2\text{-}5}$(endo) and the 9D11$^{2\text{-}5}$(tran) enhancers displayed relatively low H3K27ac in the type II neuroblast-enriched chromatin (Figure 1I), we tested if robust histone deacetylation is required for maintaining *erm* inactive in type II neuroblasts. By knocking down the function of genes that encode histone deacetylases in flies, we found that decreasing *rpd3* function specifically and reproducibly leads to loss of type II neuroblasts (Supplementary Figure 2C). To test if *rpd3* is required for self-renewal, we generated mosaic clones derived from single *rpd3* mutant type II neuroblasts (Supplementary Figures 2D-E). A wild-type clone always contained a type II neuroblast that measures approximately 10 μm in diameter (Figures 2J and 2M). In contrast, more than 50% of *rpd3* mutant type II neuroblasts displayed dramatically reduced cell diameter, and 19% of *rpd3* mutant clones lacked identifiable neuroblasts (Figures 2K-M). Over-expressing *rpd3* but not *hdac3*, which is also required for types II neuroblast self-renewal (Supplementary Figures 2F), rescued the premature differentiation phenotype in *rpd3* mutant clones (Figure 2M). These results strongly suggest that Rpd3-dependent histone deacetylation promotes type II neuroblast self-renewal. We next tested if Rpd3 is required for repressing *erm* expression in type II neuroblasts by maintaining the 9D11$^{2\text{-}5}$ enhancer in a poised sate. In agreement with our hypothesis, knocking down *rpd3* function led to robust premature activation of *9D11$^{2\text{-}5}$-GFP* in type II neuroblasts (Figures 2N-O). Furthermore, *rpd3* mutant type II neuroblasts consistently displayed low but detectable endogenous Erm expression (Figures 2P-Q). Lastly, removing *erm* function suppressed premature differentiation of *rpd3* mutant type II neuroblasts (Figure 2R). These data led us to conclude that Rpd3 is required for maintaining *erm* in an inactive state in type II neuroblasts by poising its immature INP enhancer in conjunction with Trx (Figure 2S).

Self-renewal transcriptional repressors and type II neuroblast transcriptional activators directly regulate *erm* expression by binding the immature INP enhancer

We next sought to identify specific transcription factors that function together with Rpd3 to maintain the *erm* immature INP enhancer in a poised state in type II neuroblasts. The self-renewal transcription factors Klu, Dpn and E(spl)mγ are excellent candidates because *klu* single mutant or *dpn* and *E(spl)* double mutant type II neuroblasts also display reduced diameter and prematurely differentiate, similar to *rpd3* mutant type II neuroblasts (Xiao et al., 2012; Zacharioudaki et al., 2012). Consistent with this possibility, we found that Klu, Dpn and E(spl)mγ directly bind conserved sites in the 9D11$^{2\text{-}5}$ enhancer *in vitro* (Figures 3A and 3E; Supplementary Figures 3A-C). Dpn and E(spl)mγ are evolutionarily conserved transcriptional repressors, but how Klu regulates gene expression is less clear (Kobayashi and Kageyama, 2014; Taelman et al., 2004; Zacharioudaki et al., 2012). We generated a series of *UAS* transgenes that encode Klu^{zf} (the Klu DNA-binding zinc-finger motif only), VP16::Klu^{zf} (a constitutive transcriptional activator) or ERD::Klu^{zf} (a constitutive transcriptional repressor). Over-expression of Klu^{zf} or VP16::Klu^{zf} did not lead to supernumerary neuroblast formation (Figure 3B). By contrast, over-expression of full-length Klu or ERD::Klu^{zf} triggered the formation of supernumerary neuroblasts (Figure 3B). These data indicate that Klu promotes type II neuroblast self-renewal by acting as a transcriptional repressor. We extended our analyses to examine whether Klu functions collaboratively with Dpn and E(spl)mγ to promote type II neuroblast self-renewal. Removing *dpn* or *E(spl)mγ* function strongly suppressed supernumerary type II neuroblast formation induced by *klu*

over-expression (Figure 3C). Similarly, removing *klu* function strongly suppressed the supernumerary type II neuroblast phenotype induced by *dpn* or *E(spl)mγ* over-expression (Figure 3C). Thus, Klu, Dpn and E(spl)mγ function interdependently as a transcriptional repressor network to promote type II neuroblast self-renewal.

To examine whether Klu, Dpn and E(spl)mγ promote type II neuroblast self-renewal by repressing *erm* expression through the 9D11$^{2-5}$ enhancer, we took two complimentary approaches. First, we tested if Klu and E(spl)mγ are necessary and sufficient to prevent premature *9D11$^{2-5}$-GFP* expression in type II neuroblasts. Indeed, knocking down *klu* function or removal of the *E(spl)* locus resulted in premature *9D11$^{2-5}$-GFP* expression in type II neuroblasts (Supplementary Figures 3D-G). Conversely, over-expressing *klu* or *E(spl)mγ* reduced *9D11$^{2-5}$-GFP* expression *in vivo* (Figure 3D). Second, tested if Klu, Dpn and E(spl)mγ directly repress *erm* expression by binding the 9D11$^{2-5}$ enhancer. We generated a series of mutant *9D11$^{2-5}$-GFP* transgenes where the confirmed Klu-binding site, Dpn/E(spl)-binding sites or both are mutated (Figure 3E). In contrast to the wild-type *9D11$^{2-5}$-GFP* transgene containing functional Klu-binding or Dpn/E(spl)-binding sites, the mutant *9D11$^{2-5}$-GFP* transgenes became prematurely activated in type II neuroblasts (Figures 3F-H). Furthermore, the activities of mutant *9D11$^{2-5}$-GFP* transgenes became significantly increased relative to the wild-type transgene (Figure 3I). These data led us to conclude that Klu, Dpn and E(spl)mγ function together to promote type II neuroblast self-renewal by directly repressing activation of the 9D11$^{2-5}$ enhancer (Figure 3K).

Premature expression of these mutant *9D11$^{2-5}$-GFP* transgenes strongly suggest that transcriptional activators required for their activation are bound to the *erm* immature INP enhancer in type II neuroblasts. The ETS-1 transcriptional activator PntP1 is an excellent candidate to activate the 9D11$^{2-5}$ enhancer for the following reasons. First, PntP1 is specifically expressed in type II neuroblasts and in Ase^{-} immature INPs (Figure 1A). Second, loss of *pntP1* function leads to reduced Erm expression in immature INPs as well as supernumerary type II neuroblast formation (Komori et al., 2014a; Xie et al., 2016). Indeed, we found that knocking down *pntP1* function reduced the expression of *9D11$^{2-5}$-GFP in vivo*, and the ETS-domain of PntP1 bound five of the seven putative PntP1-binding sites in the 9D11$^{2-5}$ enhancer *in vitro* (Figure 3J; Supplementary Figures 3H-I). These data strongly suggest that opposing inputs from repressors Klu, Dpn and E(spl)mγ and lineage-specific activators such as PntP1 poise the 9D11$^{2-5}$ enhancer in self-renewing type II neuroblasts to enable rapid onset of *erm* expression in immature INPs (Figure 3K).

Self-renewal transcriptional repressors function through Rpd3-mediated deacetylation of multiple histone proteins to poise the *erm* immature INP enhancer in type II neuroblasts

Our data indicate that both self-renewal transcriptional repressors and Rpd3 promote type II neuroblast self-renewal partly by maintaining the *erm* immature INP enhancer in a poised state. To test if Klu, Dpn and E(spl)mγ function through Rpd3 to promote type II neuroblast self-renewal, we generated *rpd3* mutant type II neuroblast clones over-expressing these proteins individually. Consistent with our hypothesis, removing *rpd3* function strongly suppressed the supernumerary neuroblast phenotype induced by over-expression of Klu,

Dpn or E(spl)mγ (Figures 4A-C). Thus, Klu, Dpn and E(spl)mγ function through Rpd3 to promote a type II neuroblast identity.

Rpd3 deacetylates many residues on histones, and increased H3K27ac catalyzed by CBP has been attributed to the activation of poised enhancers in vertebrates. If Klu, Dpn and E(spl)mγ function through Rpd3-dependent deacetylation of H3K27 to poise the $9D11^{2-5}$ enhancer in type II neuroblasts, the mutant $9D11^{2-5}$(tran) enhancer lacking functional Klu, Dpn and E(spl)-binding sites should exhibit increased H3K27ac as compared to the wild-type $9D11^{2-5}$(tran) enhancer. Indeed, the mutant $9D11^{2-5}$(tran) enhancer displayed elevated H3K27ac in the type II neuroblast-enriched chromatin as compared to the wild-type $9D11^{2-5}$(tran) enhancer (Supplementary Figure 4A). Thus, self-renewal repressors likely work together with Rpd3 to suppresses the acetylation of H3K27 on the $9D11^{2-5}$ enhancer in type II neuroblasts. To identify the histone acetyltransferases (HATs) required for *erm* activation, we knocked down the function of genes encoding HATs by over-expressing a collection of *UAS-RNAi* transgenes in an *erm* hypomorphic background. Contrary to expectation, knocking down the function of CBP, encoded by *nejire* (*nej*) in flies, by two independent RNAi lines suppressed the supernumerary neuroblast phenotype in the *erm* hypomorphic background (Figure 4D; Supplementary Figures 4B-C). In contrast, knocking down either *mof* or *Gcn5* had no effect on the supernumerary neuroblast phenotype, while knocking down *tip60* or *HBO1* encoded by *chameau* (*chm*) in flies, consistently increased the number of supernumerary neuroblasts in this background (Figure 4D; Supplementary Figures 4B and 4D-E). Tip60 has primarily been implicated in the acetylation of H2A and H2A.Z (also called H2A.v in *Drosophila*), whereas HBO1/Chm has been implicated in acetylation of lysine 5, 8, 12, and 16 on histone 4 (Kusch et al., 2004; McConnell et al., 2012; Miotto and Struhl, 2010; Petesch and Lis, 2012). Based on these results, we reasoned that Rpd3 likely maintains the *erm* immature INP enhancer in a poised state through continual deacetylation of multiple histone proteins. Consistently, we found *rpd3* mutant type II neuroblast clones display significantly increased acetylation at H2AK5, H2A.Z, H3K27 and H4K16 (Figures 4E-M; Supplementary Figures 4F-M). Together, these data led us to conclude that self-renewal transcriptional repressors function together with Rpd3 to poise the *erm* immature INP enhancer in type II neuroblasts through continual deacetylation of histone proteins (Figure 4N). Down-regulation of repressor activities allows a rapid burst in histone acetylation triggering *erm* expression within two-hours of immature INP birth (Figure 4O).

Elucidating and validating a functional Erm-binding sequence

To elucidate how Erm restricts the developmental potential in immature INPs, we sought to identify a functional Erm-binding sequence. We screened a collection of reporters that contain candidate Erm-binding sequences for their responses to the over-expression of a series of *erm* transgenes in *S2* cells. The $Erm^{\Delta N}$ transgenic protein is non-functional, and serves as a negative control (Janssens et al., 2014). Over-expression of VP16::Erm can exert a dominant negative effect on the supernumerary neuroblast phenotype in *erm* hypomorphic brains, most likely by activating Erm target gene expression (Janssens et al., 2014). Only the activity of the *luc* transgene bearing a putative Erm-binding sequence (referred to as the Erm response element (ErmRE) hereafter) identified by the FlyFactor survey (http://

mccb.umassmed.edu/ffs/TFdetails.php?FlybaseID=FBgn0031375) could be repressed by over-expression of Erm but activated by over-expression of VP16::Erm in *S2* cells (Figures 5A-B). Importantly, the ErmRE^{mut} reporter that contains two nucleotide substitutions in the ErmRE was no longer responsive to the expression of this collection of *erm* transgenes in *S2* cells (Figures 5A-B). We previously showed that the vertebrate homologues of Erm, FezF1 and FezF2, likely regulate target gene expression through a similar mechanism. Thus, we tested whether the Erm-binding site we identified here may act as conserved consensus binding sequence for the Fezf transcription factor family. Indeed, the zinc-finger motif of Erm as well as Fezf1 and Fezf2 bound the sequence from the wild-type but not the mutant ErmRE with a high affinity and specificity *in vitro* (Figures 5C-D; Supplementary Figure 5A). Thus, we conclude that AAAAGAGCAAC is a consensus DNA sequence recognized by the Fezf family of transcription factors from *Drosophila* to mammals.

To functionally validate the specificity of ErmRE *in vivo*, we generated flies bearing a reporter containing either the wild-type or the mutant ErmRE (Figure 5A). First, we examined the expression of these reporters in the wild-type type II neuroblast lineage, where endogenous Erm is exclusively expressed in Ase^{-} and Ase^{+} immature INPs (Figures 1A and 1C). The expression of ErmRE-GFP became down-regulated in immature INPs as compared to the type II neuroblast, and its expression remained low in INPs (Figure 5E; Supplementary Figure 5B). In contrast, the expression ErmRE^{mut}-GFP did not become down-regulated in immature INPs and INPs to a similar extent as ErmRE-GFP (Figures 5E-F; Supplementary Figure 5B). Thus, the ErmRE can be recognized and repressed by endogenous Erm. Next, we tested the response of these two reporters to the overexpression of our collection of Erm transgenes in *erm* mutant brains. Consistent with our results in *S2* cells, expression of ErmRE-GFP but not ErmRE^{mut}-GFP can be repressed by Erm over-expression, and activated by over-expression of VP16::Erm in larval brains (Figure 5G). These data led us to conclude Erm is able to bind the sequence AAAAGAGCAAC, and exert transcriptional repression of target gene expression *in vivo*.

Erm restricts the developmental potential in immature INPs by repressing *pntP1* and *grhO* transcription

To identify the direct targets that Erm represses to restrict the developmental potential in immature INPs, we searched our microarray database for genes whose transcript levels become up-regulated in *erm* null brains. We found multiple genes that encode type II neuroblast transcription factors were significantly up-regulated in *erm* mutants as compared to wild-type brains (data not shown). To distinguish direct targets from indirect targets, we examined the responsiveness of these genes to a 12-hour pulse of transgenic Erm or VP16::Erm over-expression in *erm* null brains. We found that over-expression of *erm* significantly decreases the *pntP1* and *grhO* transcript levels, but over-expression of *VP16::erm* increases their levels (Figure 6A). By contrast, over-expression of these *erm* transgenes did not have as pronounced an effect on the transcription of *pntP3*, *grhN, dpn* or *klu*, (Figure 6A). These data strongly suggest that *pntP1* and *grhO* are the direct targets of Erm.

To test if *pntP1* and *grhO* are indeed the direct targets of Erm, we generated a position weight matrix for our identified Erm-binding sequence, and found a cluster of six putative Erm-binding sites just upstream of the *pntP1* TSS and three putative Erm-binding sites just upstream of the *grhO* TSS. Consistent with the possibility that these clusters of putative Erm-binding sites may represent functional ErmREs, they are conserved in all *Drosophila* species (data not shown). More importantly, the Erm DNA-binding domain bound at least four of the sites in the *pntP1* TSS and all three sites in the *grhO* TSS (Supplementary Figures 6A-B). Lastly, a reporter containing the *pntP1* promoter with wild-type but not mutant Erm-binding sites was repressed by wild-type Erm and activated by VP16::Erm in *S2* cells (Figure 6B). Similarly, only a reporter containing the *grhO* promoter with wild-type Erm-binding sites was activated by VP16::Erm in *S2* cells (Figure 6C). Thus, we conclude Erm can directly bind upstream of the *pntP1* TSS and *grhO* TSS.

To determine if Erm is required to down-regulate the expression of *pntP1* and *grhO in vivo*, we tested whether PntP1 or GrhO becomes mis-regulated in *erm* null type II neuroblast clones. Consistent with previous reports, PntP1 was detected in type II neuroblasts and a few immature INPs, but undetectable in remaining cells of a wild-type type II neuroblast lineage (Figure 6D). By contrast, we detected ectopic PntP1 expression in all *erm* null type II neuroblast clones, but the severity of mis-regulated PntP1 expression differed among type II neuroblast lineages. In the *erm* mutant clones derived from the DL1, DM2, DM4 or DM5 type II neuroblast, PntP1 became ectopically expressed in virtually all cells (Figures 6E-F; Supplementary Figures 3C-D and 3F). In the *erm* mutant clones derived from the DL2, DM1, DM3, and DM6 type II neuroblast, PntP1 was down-regulated in immature INPs similar to wild-type clones, before becoming re-expressed in INPs as they began to revert into supernumerary neuroblasts (Supplementary Figures 6C-D and 6F; data not presented). Similar to PntP1, we found GrhO also became ectopically expressed in *erm* null type II neuroblast clones in a lineage-dependent manner (Figures 6G-I; Supplementary Figures 6C and 6E-F). Thus, we conclude that Erm directly represses PntP1 and GrhO expression in immature INPs, and that an additional partially redundant mechanism may act in parallel to Erm to regulate PntP1 and GrhO expression in a subset of type II neuroblast lineages.

We hypothesized that Erm restricts the developmental potential in immature INPs by repressing the transcription of genes important for a type II neuroblast functional identity. Thus, we tested if over-expression of *grhO* or *pntP1* in late stage (Ase^{+}) immature INPs as well as mature INPs can trigger INP reversion into supernumerary type II neuroblasts. Over-expression of either gene individually or in combination was insufficient to induce supernumerary type II neuroblasts in wild-type brains (data not presented). These results suggested that Erm likely represses additional transcriptional activators that function cooperatively with PntP1 and GrhO to promote a type II neuroblast identity. Thus, we over-expressed *grhO* or *pntP1* individually or in combination in *erm* hypomorphic brains. While over-expression of *grhO* or *pntP1* alone did not worsen the supernumerary type II neuroblast phenotype, co-expression of *grhO* and *pntP1* enhanced the supernumerary type II neuroblast phenotype in this genetic background (Figures 6J-L). Thus, Erm restricts the developmental potential in immature INPs by acting as a negative feedback regulator to repress components of the transcriptional activator network that promotes type II neuroblast self-renewal (Figure 7).

Discussion

Tissue-specific stem cells amplify the output of each division by producing intermediate progenitors that must rapidly acquire restricted developmental potential to ensure timely generation of differentiated cell types. Failure to properly restrict the developmental potential of intermediate progenitors can result in their transformation into tumor initiating cells in flies, and likely in vertebrates (Alcantara Llaguno et al., 2015; Caussinus and Gonzalez, 2005; Eroglu et al., 2014; Koe et al., 2014). Thus, elucidating how developmental potential becomes rapidly restricted in intermediate progenitors will provide critical insight into normal development as well as the tumorigenic transformation of stem cell progeny. In this study, we demonstrated that in the fly brain, Erm rapidly and stably restricts the developmental potential of intermediate progenitors through a poised negative feedback circuit (Figure 7). This highly streamlined mechanism balances continual self-renewal with rapid restriction of the developmental potential during asymmetric stem cell division. Our study demonstrates the utility of poised enhancers for rapid activation of the differentiation programs in stem cell progeny within hours of their birth. Previous studies of human and mouse embryonic stem cells revealed PRC2 is bound to the promoter of *Fezf2*, and the *Fezf2* neurogenic enhancer displays H3K4me1 and H3K27me3 (Boyer et al., 2006; Eckler et al., 2014; Rada-Iglesias et al., 2011). This suggests embryonic stem cells maintain *Fezf2* in a poised state for subsequent activation in the developing nervous system. Thus, an analogous poised circuit similar to what we describe in this study may also exist to ensure that the developmental potential is rapidly restrained in the progeny of vertebrate neural stem cells.

Histone deacetylation maintains fast-activating enhancers in a poised state in self-renewal stem cells

Accumulating evidence suggests that H3K27me3 is replaced by H3K27ac during the activation of a poised enhancer, leading to a model that the trimethylation of H3K27 precludes CBP-catalyzed acetylation to prevent premature activation of these poised enhancers in stem cells (Calo and Wysocka, 2013; Heinz et al., 2015; Zentner et al., 2011). However, direct evidence demonstrating the transition from H3K27me3 to H3K27ac is the cause rather than the consequence of poised enhancer activation is lacking. In addition, whether stem cells require PRC2 to prevent activation of the genes that will be expressed in their immediate progeny in a physiological context also remains unclear.

We discovered that both the *erm* TSS and the endogenous *erm* immature INP enhancer display a poised chromatin signature in type II neuroblasts (Figures 1G and 1I). However, robust histone deacetylation catalyzed by Rpd3 rather than H3K27 trimethylation deposited by PRC2 plays the leading role in preventing premature *erm* activation in self-renewing type II neuroblasts (Figure 2). Rpd3 most likely functions together with self-renewal transcriptional repressors Dpn, Klu and E(spl)mγ to continually deacetylate histone proteins on the *erm* immature INP enhancer, and prevent premature *erm* activation in type II neuroblasts (Figure 3-4). Rapid down-regulation of the activities of these self-renewal transcriptional repressors in immature INPs and possibly additional factors alleviates Rpd3-dependent repression triggering activation of the *erm* immature INP enhancer. Thus, our

results provide compelling evidence of an under-appreciated, histone deacetylation-mediated mechanism that orchestrates precise activation of master regulators of differentiation through their poised enhancers during asymmetric cell division. An analogous mechanism most likely exists in vertebrate embryonic stem cells where the poised state of many neuronal genes that display a bivalent chromatin signature is regulated by HDACs rather than PRC2 (McGann et al., 2014). We propose fast-activating poised enhancers rely primarily on continual Rpd3-mediated deacetylation of multiple histone proteins to remain inactive in stem cells. In addition, our results indicate that loss of H3K27me3 during activation of these enhancers is likely the consequence of reduced Rpd3 activity, and that PRC2 has a more nuanced role during the regulation of fast-activating poised enhancers than directly maintaining repression per se.

Regulation of rapid transition from a poised to an active chromatin state in differentiating stem cell progeny

Following asymmetric stem cell division, the differentiating progeny must rapidly activate differentiation programs. Thus, the chromatin at loci that harbor master regulators of differentiation must be the first to transition from an inactive state to an active state in the stem cell progeny destined to differentiate. However, very little is known about these initial changes in chromatin dynamics.

By investigating how the *erm* immature INP enhancer is regulated in the type II neuroblast lineage, we made two discoveries about the mechanism that enables rapid activation of a master regulator of differentiation in differentiating stem cell progeny. First, self-renewal transcriptional repressors function antagonistically to type II neuroblast-specific transcriptional activators to maintain the *erm* immature INP enhancer in a poised chromatin state through histone deacetylation (Figure 3; Supplementary Figure 3). Second, multiple HATs including Tip60 and HBO1/Chm likely contribute to rapid *erm* activation in immature INPs by acetylating multiple histone proteins (Figures 4D-O). Demonstrating a direct connection between histone acetylation by Tip60 and HBO1/Chm and activation of the *erm* immature INP enhancer will be a key future experiment to confirm our observations. Our data raised an intriguing model that type II neuroblast-specific transcriptional activators such as PntP1 are required for the activity of these HATs on the *erm* immature INP enhancer. This model would explain why *erm* is exclusively activated in the progeny of a type II neuroblast, despite being marked by H3K4me2 in both type I and type II neuroblasts (Figures 1G-H). We propose the robust histone deacetylase activity of Rpd3 counteracts the activity of multiple HATs to maintain the poised state of the *erm* immature INP enhancer in type II neuroblasts. Rapid down-regulation of self-renewal transcriptional repressors in immature INPs alleviates Rpd3-dependent deacetylation, permitting acetylation of multiple histone proteins on the *erm* immature INP enhancer. This proposed mechanism serves as the very first step during the exit from stemness and the commitment to differentiation in newly born intermediate progenitors, raising the exciting possibility that other tissue-specific stem cell types may utilize similar fast-activating poised enhancers to initiate differentiation programs in their progeny.

Regulation of restricted developmental potential in intermediate progenitors

erm is a unique, fast-activating poised gene whose expression is precisely specified in immature INPs to restrict their developmental potential, and this study has uncovered key mechanisms that dictate the timing of *erm* activation (Figures 2-3). To achieve this specific temporal expression pattern, additional post-transcriptional mechanisms must also exit to ensure that the Erm protein does not persist into INPs. Elucidating the mechanisms that ensure timely turn-over of the Erm protein will likely improve our understanding of the regulation of developmental potential in immature INPs.

Restricting the developmental potential in uncommitted intermediate progenitors involves restraining the mechanisms that endow stem cells with their unique functional properties. By identifying AAAAGAGCAAC as a consensus DNA-binding sequence of the Fezf family of transcription factors (Figure 5), we were able to show that Erm directly binds variations of this sequence in the promoters of *pntP1* and *grhO* to repress their expression in immature INPs (Figure 6). Thus, Erm restricts the developmental potential in immature INPs by directly repressing components of the type II neuroblast transcription factor network (Figure 7). Interestingly, PntP1 is also required for activating the *erm* immature INP enhancer, and loss of *pntP1* function leads to supernumerary type II neuroblast formation mimicking the *erm* null phenotype (Komori et al., 2014a). This suggests Erm acts as part of a negative feedback circuit to repress components of the stem cell transcription factor network, thereby restricting the developmental potential of INPs while simultaneously dismantling the mechanisms that promote the activation of its own enhancer (Figure 7). Identifying similar regulatory circuits that balance self-renewal with differentiation in other stem cell lineages will require in-depth knowledge of (1) the core stem cell transcription factor network, (2) the functional consequence of the binding of specific transcription factors to the poised enhancers of pro-differentiation genes (i.e activation vs. repression), and (3) the mechanisms that alter the activity of components of the stem cell transcription factor network in stem cell progeny. Ultimately, understanding these poised regulatory circuits will facilitate the precise generation of specific differentiated cell types for regenerative medicine, and provide insight into how specific oncogenic lesions contribute to the formation and growth of stem cell and intermediate progenitor derived tumors.

Experimental Model and Subject Details

VanGlow Reporter Plasmids

To create the VanGlow series of reporter vectors (Supplementary Figures 1A-B), synthetic DNA fragments encoding a GFP::Luciferase(nls) or mCherry::Renilla(nls) (codon optimized for expression in *Drosophila*), and a yeast transcriptional terminator flanked by HindIII sites were generated by GeneArt™ (Thermofisher scientific). These constructs were then cloned into the pBPGw (Addgene #17574) and pBPGUw (Addgene #17575) vectors using the HindIII sites to replace GAL4, generating the VanGlow-GL (Addgene #83342), VanGlow-RR (Addgene #83343), VanGlow-GL-DSCP (Addgene #83338), and VanGlow-RR-DSCP (Addgene #83339) vectors. The 9D11 reporter series was generated by standard Gateway® cloning of regions of the 9D11 enhancer into the VanGlow-GL-DSCP plasmid, and in some cases the VanGlow-RR-DSCP plasmid as well. The mutant $9D11^{2\text{-}5}$ and ErmRE fragments

were generated by IDT as gBlocks® and inserted into the VanGlow-GL-DSCP plasmid by Gateway® cloning. Overlap extension or "sewing" PCR was used to mutagenize the Erm-binding sites in the *pntP1* and *grhO* promoters, changing the G in the fifth position of each site to an A, and the A in the ninth position to a G (Supplementary Figures 6A-B). Standard Gateway® cloning was used to insert the wild type and mutant *pntP1* and *grhO* promoters into the VanGlow-GL vector. Primers used for PCR amplification of regions of 9D11 as well as the *pntP1* and *grhO* promoters are listed in Table S1.

Fly Genetics and Transgenes

Fly crosses were carried out in 6oz plastic bottles, and eggs were collected on apple caps in 8-hour intervals. The following day, newly hatched larvae were transferred to corn meal caps, and grown at 25°C. To relieve repression of Gal4 by *tub-Gal80^{ts}* and induce UAS-transgene expression, larvae were shifted to 33°C. To generate MARCM clones, a pulse of *hs-flp* expression was induced in first instar larvae by floating their meal caps in a 38°C water bath for an hour and twenty minutes. Unless otherwise indicated, larval brains were dissected and processed for imaging 72hrs after clone induction. The 9D11- and ErmRE-VanGlow reporter flies were generated by ϕC31 integrase-mediated transgenesis into the PBAC (yellow[+]-attP-3B)VK00033 docking site (Bischof and Basler, 2008). DNA injections were carried out by BestGene Inc., and transgenic flies were identified in the F1 generation based on their yellow eye color.

S2 Cells

S2 Cells were maintained in a 25°C incubator and grown in 10cm Corning® tissue culture plates in Schneider's *Drosophila* media supplemented with 10% bovine growth serum. Every 3-5 days cells were passaged and split to 30% confluency.

Method Details

Immunofluorescence Staining

Third instar larval brains were dissected in PBS and fixed in 100 mM PIPES (pH 6.9), 2 mM EGTA, 0.3% Triton X-100, 1 mM $MgSO_4$ containing 4% formaldehyde for 23 minutes on a nutator at room temp. To stop fixation, samples were washed with PBS containing 0.3% Triton X-100 (PBST) (2X quick wash, followed by 2X 20 min wash). Primary antibodies were diluted in PBST and staining was carried out on a nutator at room temp for three hours, except when using rabbit anti-Erm or rabbit anti-PntP1, in which case samples were incubated on a nutator at 4°C overnight. Samples were then washed with PBST on a nutator at room temp, and when desired, Alexa Fluor-conjugated phalloidin was added during a 30 min incubation. Secondary antibody staining was carried out in PBST on a nutator at 4°C overnight. Larval brains were then washed with PBST and stored in Prolong™ Gold antifade reagent (Life technologies). Information on antibodies and dilution factors used for staining are included in the Key Resource Table. Confocal images were acquired on a Leica SP5 scanning confocal microscope.

Time-lapse Imaging of Type II Neuroblasts

Time-lapse experiments were performed on third instar transgenic animals bearing a single copy of the *9D11$^{2-5}$-GFP::Luc(nls)* transgene and the *9D11$^{2-5\ mut\ Klu/Dpn/E(spl)}$-mCherry::Ren(nls)* transgene (included to mark type II lineages). Larval brain explants were cultured in D22 media (pH 6.95) supplemented with 7.5% bovine growth serum and 10mM ascorbic acid. Time-lapse acquisition was performed on a Leica SP8 laser scanning confocal microscope equipped with 488 nm and 543 nm laser lines used for GFP and RFP excitation respectively. GFP/RFP z-stack series (8-10 focal planes with 1.5 µm spacing) were acquired at 30s intervals using sequential line scanning mode.

Acquired images series were processed using Fiji (Schindelin et al., 2012). To compensate for moderate fluorophore photobleaching, mean whole volume fluorescence intensity was determined for the first (GFP^{t0} and RFP^{t0} and last time point (GFP^{tn} and RFP^{tn}) in each time-lapse series. The bleaching coefficient b^{coeff} was calculated separately for each fluorophore channel as GFP^{t0}/GFP^{tn} and RFPt0/RFP^{tn}. For composition of the time-lapse movies, image intensity levels were linearly scaled for each timepoint (tx) and fluorophore channel using the factor $b^{coeff} * (tx / tn)$. To reduce pixel noise, a Gaussian filter (sigma=1) was applied to each image after bleaching correction.

Chromatin Immunoprecipitation

ase>aPKC^{CAAX} or *brat$^{11/150}$* mutant larvae were aged for 5-7 days at 33°C. Grou ps of 100 brains were dissected directly into Schneider's medium then fixed in cross-linking solution (1% methanol free-formaldehyde, 50mM HEPES(pH 8), 1mM EDTA, 0.5mM EGTA, 100mM NaCl) for 10 min. Fixation was stopped by washing twice with Glycine solution (0.125 M, 0.01% Triton X-100) in PBS at room temperature for 5 min. Samples were then washed twice with wash buffer A (10mM HEPES(pH 7.6), 10mM EDTA, 0.5mM EGTA, 0.25% Triton X-100) and twice with wash buffer B (10mM HEPES(pH 7.6), 1mM EDTA, 0.5mM EGTA, 200mM NaCl, and 0.01% Triton X-100) and then snap frozen in liquid nitrogen.

To obtain more than 2×10^6 supernumerary neuroblasts per ChIP sample, 400 brains were pooled in 200ul SDS lysis buffer (1% SDS, 1 mM PMSF, 50 mM Tris–HCl pH8.1, 10 mM EDTA, 10mM Na-butyrate) containing proteinase inhibitors (Roche, Basel, Switzerland), and homogenized using a glass mortar and pestle. The nuclear extracts were disrupted by sonication (60 cycles of sonicating for 30 s with 30 s intervals) using a Diagenode, Bioruptor xL. The sonicated chromatin was diluted in 5X the volume of ChIP dilution buffer (0.01% SDS, 1.1% Trition X-100, 1.2 mM EDTA, 16.7 mM Tris–HCl pH8.1, 167 mM NaCl), and ten percent of the volume used in each ChIP sample was stored at −30°C as an INPUT control. The rest of the chromatin was split into nonstick 1.5 ml microfuge tubes and incubated with primary antibodies on a rotator at 4°C overnight. Samples were then incubated with 60 µl Protein A agarose/salmon sperm DNA beads (16–157; Millipore, Billerica, MA) on a rotator at 4°C for 4-6 hours, washed twice with low salt immune complex wash buffer (0.1% SDS, 1% TritonX-100, 2 mM EDTA, 20 mM Tris–HCl pH8.1, 150 mM NaCl) for 5 min, once with high salt immune complex wash buffer (0.1% SDS, 1% TritonX-100, 2 mM EDTA, 20 mM Tris–HCl pH8.1, 500 mM NaCl) for 5 min, once with

LiCl immune complex wash buffer (0.25 M LiCl, 1% NP40, 1% deoxycholate, 1 mM EDTA, 10 mM Tris–HCl pH8.1) for 5 min, and twice with TE buffer. Chromatin was eluted from beads in elution buffer (10% SDS, 0.1M $NaHCO_3$) for 5 min at 45°C on a shaker. Cross-linking of chromatin–protein complex was reverted at 65°C overnight. Samples were treated with RNase A at 37°C for 1 hr and incubated with 2 μg of proteinase K at 45°C for 2 hr. Samples were cleaned up by phenol:chloroform extraction followed by EtOH precipitation, re-suspended in 75 μl of water, and 1.5 μl of sample was used per 15 μl qPCR reaction. Specific primer sets used for ChIP qPCR are listed in Table S1.

Luciferase Assays

S2 Cells- to facilitate constitutive expression in S2 cells, 3XHA-C-terminal-tagged *erm, erm*$^{\Delta N}$ and *VP16-erm* were cloned into the pAc5.1/V5-His-A expression vector (ThermoFisher Scientific). For each transfection condition a total of 0.5 mL of 1×10^7 S2 cells/mL were seeded in 12-well plates in serum free media. To prepare the DNA for transfection 700ng pcDNA3, 100ng of VanGlow luciferase reporter plasmid, 150ng of the pAc5.1 expression vector and 10ng of pRL-CMV, which served as an internal control, where suspended in 50 μl Schneider's media and incubated with 3 μl FuGENE HD transfection reagent (Promega) for 30 min at room temp, then added to S2 cells in a dropwise manner. Six hours later, bovine growth serum was added to the transfected cells to a final concentration of 10%. Cell lysis and dual luciferase assays were performed 24 hours after transfection using standard procedures. ***Drosophila* Brains-** single brains were dissected directly into 65 μl of Passive lysis buffer (Promega) and triturated to homogenize tissue, except for the analysis of ErmRE reporters where four brains were pooled per sample. Luciferase assays were performed using standard procedures.

Protein Expression and Purification

The DNA-binding domains of Erm (amino acids 316-482), Fezf1 (258-424), Fezf2 (270-436), Klu (560-708), PntP1 (499-604), and E(spl)mγ (2-86) were cloned into pMALc2x (New England Biolabs). Following induction, MBP-fusion proteins were purified from *E. coli* in column buffer (20 mM Hepes (pH 7.6), 0.2 M NaCl, 1 mM EDTA, 10 mM β-mercaptoethanol, 2 mM PMSF) using amylose resin (New England Biolabs). After washing, protein was eluted with 20 mM maltose in elution buffer (20 mM Hepes (pH 7.6), 100 mM NaCl, 1 mM EDTA, 10% glycerol). Dpn (28-106) was cloned into pGEX6p1. GST-Dpn was purified in column buffer (25 mM Hepes (pH 7.6), 0.15 M NaCl, 10% glycerol, 1 mM EDTA, 10 mM β-mercaptoethanol, 2 mM PMSF) using Glutathione HiCap Matrix (Qiagen). After washing, protein was eluted with 20 mM glutathione in column buffer. Protein concentrations were measured by Coomassie stained SDS-PAGE gels. Known concentrations of bovine serum albumin were used as a standard or proteins were standardized to previously determined concentrations of proteins from an earlier preparation.

Electromobility Shift Assays

40fmol Cy5-labeled oligonucleotide probe and 75ng poly(dI-dC) were used in each reaction. Amounts of recombinant protein used per reaction were as follows: 10 pmol MBP-Klu$^{560\text{-}708}$, 0.25 pmol MBP-PntP1$^{499\text{-}604}$, 5 pmol MBP-E(spl)$^{2\text{-}86}$, 8 pmol GST-Dpn$^{28\text{-}106}$,

1-8 pmol MBP-Erm$^{316-482}$, 1-8 pmol MBP-Fezf1$^{258-424}$,1-8 pmol MBP-Fezf2$^{270-436}$. For competition experiments, unlabeled competitor oligonucleotide probes were used at 10x, 250x, and 500x the concentration of the Cy5-labeled probe (see Supplemental tables 2 & 3 for sequences). All samples were incubated on ice for 20 min and electrophoresed for 35 min at 150 V and 4°C in 4% polyacrylamide gels (29:1). The sequence of the Cy5-labeled probes containing a canonical transcription factor binding site were as follows, with the DNA-binding element in bold and the bases substituted to mutate the binding sequence underlined: Erm/Fezf: TGTCAGTG**AAAAGAGCAAC**TAGCAACG, Dpn/E(spl): AATCGCAGG**ATCGCGTGTC**AACAACCG, Klu: ATGATCGGC**ACACCGACGC**AGGATCCT, PntP1: ATATAATTA**ACCGGAAGCGC**GGCACAC.

qPCR analysis of transcript abundance

Total RNA was extracted from 40-50 third instar wild type or *erm* mutant brains following the standard Trizol RNA isolation protocol (Life technologies, Grand Island, NY) and cleaned by the RNeasy kit (Qiagen, Venlo, Netherlands). First strand cDNA was synthesized from the extracted total RNA using First Strand cDNA Synthesis Kit for RT-PCR (AMV) (Roche, Basel, Switzerland). qPCR was performed using ABsolute QPCR SYBR Green ROX Mix (Thermo Fisher Scientific Inc., Waltham, MA). Relative transcript abundance was determined by the comparative CT method using *Rp49* as a normalizer gene. Specific primer sets used for qPCR are listed in Table S1.

Quantification and Statistical Analysis

To quantify the live-cell imaging of the 9D11$^{2-5}$-GFP reporter in type II neuroblast lineages Image J was used to determine the pixel intensities of mCherry and GFP in the immature INP nucleus at various times after their birth. The best-fit line for the average GFP pixel intensity/time is given by the equation:

$$\mathrm{L}/\left(1+\mathrm{e}\hat{}\left(-\mathrm{k}\left(\mathrm{x}-\mathrm{x0}\right)\right)\right)+\mathrm{A}$$

L=69.6303, k=0.0467, x0=99.2329 and A=13.2415. x0 is the midpoint of the curve, and indicates the time (min) at which GFP reaches half the maximal intensity in the immature INP nucleus ($t_{1/2max}$GFP).

The Image J software was also used to quantify the expression of the ErmRE-GFP transgene and the global levels of histone protein acetylation (Figure 4M, Supplementary Figure 5B). Dpn single channel confocal images where used to assign the area the type II neuroblast or INP nucleus, and the pixel intensities of GFP or histone protein acetylation were assessed in the same optical section.

Microsoft Excel 2010 and Graph Pad Prism were used for data compilation and graphical representation, all bar graphs line graphs and dot plots are represented as mean ± standard deviation. All statistical analysis was done using a two-tailed Student's T-test, a p-value ≤ 0.05 was deemed significant as indicated by a star (*).

Supplementary Material

Refer to Web version on PubMed Central for supplementary material.

Acknowledgement

We thank Drs. S. Bray, C. Delidakis, J. Knoblich and S. Zhu for providing us reagents. We thank Drs. S. Barolo, K. Cadigan and Y. Dou, Ms. J. Xu, Mr. John Damrath and Mr. Han Xu for technical advice and support on the enhancer analysis and chromatin immunoprecipitation experiments. We thank members of the Buttitta lab, Drs. P. Harte, F. Tie, T Kerppola, Y. Yamashita, Mr. Dylan Farnsworth, and the members of the Lee lab for helpful discussion. We thank the Bloomington *Drosophila* Stock Center and the Vienna *Drosophila* RNAi Center for fly stocks. We thank BestGene Inc. for generating the transgenic fly lines. D. H. J. was supported by a Cellular and Molecular Biology training grant (T32-GM007315). This work is currently supported by NIH grants (R01GM092818 and R01NS077914).

References

Alcantara Llaguno SR, Wang Z, Sun D, Chen J, Xu J, Kim E, Hatanpaa KJ, Raisanen JM, Burns DK, Johnson JE, et al. Adult Lineage-Restricted CNS Progenitors Specify Distinct Glioblastoma Subtypes. Cancer Cell. 2015; 28:429–440. [PubMed: 26461091]

Almeida MS, Bray SJ. Regulation of post-embryonic neuroblasts by Drosophila Grainyhead. Mech Dev. 2005; 122:1282–1293. [PubMed: 16275038]

Bayraktar OA, Doe CQ. Combinatorial temporal patterning in progenitors expands neural diversity. Nature. 2013; 498:449–455. [PubMed: 23783519]

Bello B, Holbro N, Reichert H. Polycomb group genes are required for neural stem cell survival in postembryonic neurogenesis of Drosophila. Development. 2007; 134:1091–1099. [PubMed: 17287254]

Bello BC, Izergina N, Caussinus E, Reichert H. Amplification of neural stem cell proliferation by intermediate progenitor cells in Drosophila brain development. Neural Develop. 2008; 3:5.

Berger C, Harzer H, Burkard TR, Steinmann J, van der Horst S, Laurenson AS, Novatchkova M, Reichert H, Knoblich JA. FACS purification and transcriptome analysis of drosophila neural stem cells reveals a role for Klumpfuss in self-renewal. Cell Rep. 2012; 2:407–418. [PubMed: 22884370]

Betschinger J, Mechtler K, Knoblich JA. Asymmetric segregation of the tumor suppressor brat regulates self-renewal in Drosophila neural stem cells. Cell. 2006; 124:1241–1253. [PubMed: 16564014]

Bischof J, Basler K. Recombinases and their use in gene activation, gene inactivation, and transgenesis. Methods Mol Biol. 2008; 420:175–195. [PubMed: 18641947]

Blackledge NP, Rose NR, Klose RJ. Targeting Polycomb systems to regulate gene expression: modifications to a complex story. Nat Rev Mol Cell Biol. 2015; 16:643–649. [PubMed: 26420232]

Boone JQ, Doe CQ. Identification of Drosophila type II neuroblast lineages containing transit amplifying ganglion mother cells. Dev Neurobiol. 2008; 68:1185–1195. [PubMed: 18548484]

Bowman SK, Rolland V, Betschinger J, Kinsey KA, Emery G, Knoblich JA. The Tumor Suppressors Brat and Numb Regulate Transit-Amplifying Neuroblast Lineages in Drosophila. Dev Cell. 2008; 14:535–546. [PubMed: 18342578]

Boyer LA, Plath K, Zeitlinger J, Brambrink T, Medeiros LA, Lee TI, Levine SS, Wernig M, Tajonar A, Ray MK, et al. Polycomb complexes repress developmental regulators in murine embryonic stem cells. Nature. 2006; 441:349–353. [PubMed: 16625203]

Calo E, Wysocka J. Modification of enhancer chromatin: what, how, and why? Mol Cell Biol. 2013; 49:825–837.

Caussinus E, Gonzalez C. Induction of tumor growth by altered stem-cell asymmetric division in Drosophila melanogaster. Nat Genet. 2005; 37:1125–1129. [PubMed: 16142234]

Chen L, Zheng J, Yang N, Li H, Guo S. Genomic selection identifies vertebrate transcription factor Fezf2 binding sites and target genes. J Biol Chem. 2011; 286:18641–18649. [PubMed: 21471212]

Chen R, Nishimura MC, Bumbaca SM, Kharbanda S, Forrest WF, Kasman IM, Greve JM, Soriano RH, Gilmour LL, Rivers CS, et al. A hierarchy of self-renewing tumor-initiating cell types in glioblastoma. Cancer Cell. 2010; 17:362–375. [PubMed: 20385361]

Eckler MJ, Larkin KA, McKenna WL, Katzman S, Guo C, Roque R, Visel A, Rubenstein JL, Chen B. Multiple conserved regulatory domains promote Fezf2 expression in the developing cerebral cortex. Neural Dev. 2014; 9

Eroglu E, Burkard TR, Jiang Y, Saini N, Homem CC, Reichert H, Knoblich JA. SWI/SNF complex regulates Prdm protein Hamlet to ensure lineage directionality in Drosophila neural stem cells. Cell. 2014; 156:1259–1273. [PubMed: 24630726]

Haenfler JM, Kuang C, Lee CY. Cortical aPKC kinase activity distinguishes neural stem cells from progenitor cells by ensuring asymmetric segregation of Numb. Dev Biol. 2012; 365:219–228. [PubMed: 22394487]

Heinz S, Romanoski CE, Benner C, Glass CK. The selection and function of cell type-specific enhancers. Nat Rev Mol Cell Biol. 2015; 16:144–154. [PubMed: 25650801]

Janssens DH, Komori H, Grbac D, Chen K, Koe CT, Wang H, Lee CY. Earmuff restricts progenitor cell potential by attenuating the competence to respond to self-renewal factors. Development. 2014; 141:1036–1046. [PubMed: 24550111]

Janssens DH, Lee CY. It takes two to tango, a dance between the cells of origin and cancer stem cells in the Drosophila larval brain. Semin Cell Dev Biol. 2014

Kaspar M, Schneider M, Chia W, Klein T. Klumpfuss is involved in the determination of sensory organ precursors in Drosophila. Dev Biol. 2008; 324:177–191. [PubMed: 18831969]

Kobayashi T, Kageyama R. Expression dynamics and functions of Hes factors in development and diseases. Curr Top Dev Biol. 2014; 110:263–283. [PubMed: 25248479]

Koe CT, Li S, Rossi F, Wong JJ, Wang Y, Zhang Z, Chen K, Aw SS, Richardson HE, Robson P, et al. The Brm-HDAC3-Erm repressor complex suppresses dedifferentiation in Drosophila type II neuroblast lineages. Elife. 2014; 3:e01906. [PubMed: 24618901]

Komori H, Xiao Q, Janssens DH, Dou Y, Lee CY. Trithorax maintains the functional heterogeneity of neural stem cells through the transcription factor Buttonhead. Elife. 2014a; doi: 10.7554/eLife.03502

Komori H, Xiao Q, McCartney BM, Lee CY. Brain tumor specifies intermediate progenitor cell identity by attenuating β-catenin/Armadillo activity. Development. 2014b; 141

Kusch T, Florens L, Macdonald WH, Swanson SK, Glaser RL, Yates J.R.r. Abmayr SM, Washburn MP, Workman JL. Acetylation by Tip60 is required for selective histone variant exchange at DNA lesions. Science. 2004; 306:2084–2087. [PubMed: 15528408]

Lee CY, Robinson KJ, Doe CQ. Lgl, Pins and aPKC regulate neuroblast self-renewal versus differentiation. Nature. 2006; 439:594–598. [PubMed: 16357871]

Li X, Xie Y, Zhu S. Notch maintains Drosophila type II neuroblasts by suppressing expression of the Fez transcription factor Earmuff. Development. 2016; 143:2511–2521. [PubMed: 27151950]

McConnell KH, Dixon M, Calvi BR. The histone acetyltransferases CBP and Chameau integrate developmental and DNA replication programs in Drosophila ovarian follicle cells. Development. 2012; 139:3880–3890. [PubMed: 22951641]

McGann JC, Oyer JA, Garg S, Yao H, Liu J, Feng X, Liao L, Yates J.R.r. Mandel G. Polycomb- and REST-associated histone deacetylases are independent pathways toward a mature neuronal phenotype. Elife. 2014; 3

Miotto B, Struhl K. HBO1 histone acetylase activity is essential for DNA replication licensing and inhibited by Geminin. Mol Cell. 2010; 37:57–66. [PubMed: 20129055]

Neumüller RA, Richter C, Fischer A, Novatchkova M, Neumüller KG, Knoblich JA. Genome-wide analysis of self-renewal in Drosophila neural stem cells by transgenic RNAi. Cell Stem Cell. 2011; 8:580–593. [PubMed: 21549331]

Paridaen JT, Huttner WB. Neurogenesis during development of the vertebrate central nervous system. EMBO Rep. 2014; 15:351–364. [PubMed: 24639559]

Petesch SJ, Lis JT. Activator-induced spread of poly(ADP-ribose) polymerase promotes nucleosome loss at Hsp70. Mol Cell. 2012; 45:64–74. [PubMed: 22178397]

Pfeiffer BD, Jenett A, Hammonds AS, Ngo TT, Misra S, Murphy C, Scully A, Carlson JW, Wan KH, Laverty TR, et al. Tools for neuroanatomy and neurogenetics in Drosophila. Proc Natl Acad Sci U S A. 2008; 105:9715–9720. [PubMed: 18621688]

Rada-Iglesias A, Bajpai R, Swigut T, Brugmann SA, Flynn RA, Wysocka J. A unique chromatin signature uncovers early developmental enhancers in humans. Nature. 2011; 470:279–283. [PubMed: 21160473]

Rickels R, Hu D, Collings CK, Woodfin AR, Piunti A, Mohan M, Herz HM, Kvon E, Shilatifard A. An Evolutionary Conserved Epigenetic Mark of Polycomb Response Elements Implemented by Trx/MLL/COMPASS. Mol Cell. 2016; 63:318–328. [PubMed: 27447986]

Schindelin J, Arganda-Carreras I, Frise E, Kaynig V, Longair M, Pietzsch T, Preibisch S, Rueden C, Saalfeld S, Schmid B, et al. Fiji: an open-source platform for biological-image analysis. Nat Methods. 2012; 9:676–682. [PubMed: 22743772]

Taelman V, Van Wayenbergh R, Sölter M, Pichon B, Pieler T, Christophe D, Bellefroid EJ. Sequences downstream of the bHLH domain of the Xenopus hairy-related transcription factor-1 act as an extended dimerization domain that contributes to the selection of the partners. Dev Biol. 2004; 276:47–63. [PubMed: 15531363]

Viktorin G, Riebli N, Popkova A, Giangrande A, Reichert H. Multipotent neural stem cells generate glial cells of the central complex through transit amplifying intermediate progenitors in Drosophila brain development. Dev Biol. 2011; 356:553–565. [PubMed: 21708145]

Wallace K, Liu TH, Vaessin H. The pan-neural bHLH proteins DEADPAN and ASENSE regulate mitotic activity and cdk inhibitor dacapo expression in the Drosophila larval optic lobes. Genesis. 2000; 26:77–85. [PubMed: 10660675]

Weng M, Golden KL, Lee CY. dFezf/Earmuff maintains the restricted developmental potential of intermediate neural progenitors in Drosophila. Dev Cell. 2010; 18:126–135. [PubMed: 20152183]

Weng M, Lee CY. Keeping neural progenitor cells on a short leash during Drosophila neurogenesis. Curr Opin Neurobiol. 2011; 21:36–42. [PubMed: 20952184]

Xiao Q, Komori H, Lee CY. klumpfuss distinguishes stem cells from progenitor cells during asymmetric neuroblast division. Development. 2012; 139:2670–2680. [PubMed: 22745313]

Xie Y, Li X, Deng X, Hou Y, O'Hara K, Urso A, Peng Y, Chen L, Zhu S. The Ets protein Pointed prevents both premature differentiation and dedifferentiation of Drosophila intermediate neural progenitors. Development. 2016; 143:3109–3118. [PubMed: 27510969]

Xie Y, Li X, Zhang X, Mei S, Li H, Urso A, Zhu S. The Drosophila Sp8 transcription factor Buttonhead prevents premature differentiation of intermediate neural progenitors. Elife. 2014; 3

Zacharioudaki E, Magadi SS, Delidakis C. bHLH-O proteins are crucial for Drosophila neuroblast self-renewal and mediate Notch-induced overproliferation. Development. 2012; 139:1258–1269. [PubMed: 22357926]

Zentner GE, Tesar PJ, Scacheri PC. Epigenetic signatures distinguish multiple classes of enhancers with distinct cellular functions. Genome Res. 2011; 21:1273–1283. [PubMed: 21632746]

Zhang S, Li J, Lea R, Vleminckx K, Amaya E. Fezf2 promotes neuronal differentiation through localised activation of Wnt/β-catenin signalling during forebrain development. Development. 2014; 141:4794–4805. [PubMed: 25468942]

Zhu S, Barshow S, Wildonger J, Jan LY, Jan YN. Ets transcription factor Pointed promotes the generation of intermediate neural progenitors in Drosophila larval brains. Proc Natl Acad Sci U S A. 2011; 108:20615–20620. [PubMed: 22143802]

Highlights

-Rpd3 not PRC2 maintains the poised *erm* immature INP enhancer inactive in neuroblasts

-Rapid downregulation of self-renewal factors triggers *erm* expression in immature INPs

-Acetylation of multiple histone proteins activates *erm* expression in immature INPs

-Erm limits developmental potential by repressing neuroblast transcriptional activators

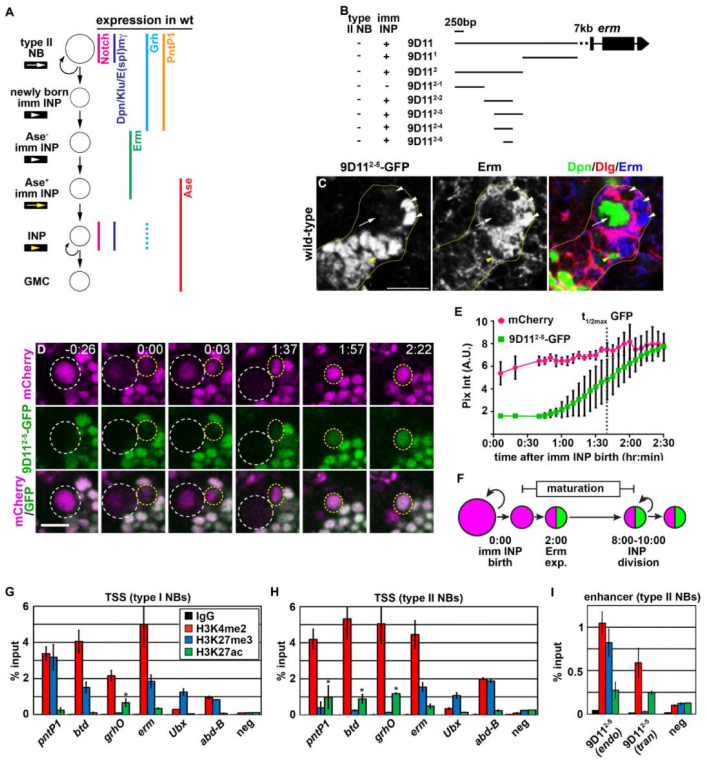

Figure 1. The 9D11$^{2-5}$ enhancer recapitulates endogenous *erm* activation in immature INPs, and is maintained in a poised state in type II neuroblasts

(A) Diagram showing the expression patterns of transcription factors in the type II neuroblast lineage. The color scheme of arrows and arrowheads used to identify various cell types in the type II neuroblast lineage in all figures is shown. The dotted line indicates that the expression is only detected in a subset of type II neuroblast lineages. (B) A summary of a subset of reporters used for mapping a minimal *erm* immature INP enhancer in the 9D11 region. (C) The expression of the *9D11$^{2-5}$-GFP::Luc(nls)* transgene (abbreviated as *9D11$^{2-5}$-GFP* in all figures) and endogenous Erm in immature INPs. (D) Live-cell analyses of the activation of *9D11$^{2-5}$-GFP* (green) in a type II neuroblast lineage marked with mCherry(nls) (magenta). 0:00 indicates the birth of an immature INP. White dotted line: type II neuroblast, Yellow dotted line: newly born immature INP. Scale bar here and throughout the manuscript: 10 μm unless otherwise noted. (E) The relative pixel intensity of mCherry and 9D11$^{2-5}$-GFP in the immature INP nucleus; $t_{1/2max}$ is the time to achieve 50% of the maximum GFP intensity in the immature INP (N = 11 immature INPs from 5 brains). All dot plots and bar graphs here and throughout the manuscript are represented as mean ± SD. (F) A schematic summary of 9D11$^{2-5}$-GFP (green) activation during INP maturation in a type II neuroblast lineage marked by mCherry (magenta). (G-H) ChIP analysis of the transcription start sites (TSS) of the indicated genes in the type I neuroblast-enriched or type II neuroblast-enriched chromatin (N ≥ 3 replicates). Statistical significance of H3K27ac in the ChIP experiments was determined using a student's t-test to compare enrichment over the IgG control relative the negative control region of the genome (neg). *: P-value here and throughout the manuscript is ≤ 0.05. (I) ChIP analysis of the endogenous 9D11$^{2-5}$ enhancer

(9D11$^{2\text{-}5}$(endo)) and the 9D11$^{2\text{-}5}$ enhancer in the *9D11$^{2\text{-}5}$-GFP* transgene (9D11$^{2\text{-}5}$(tran)) in the type II neuroblast-enriched chromatin (N ≥ 3 replicates).

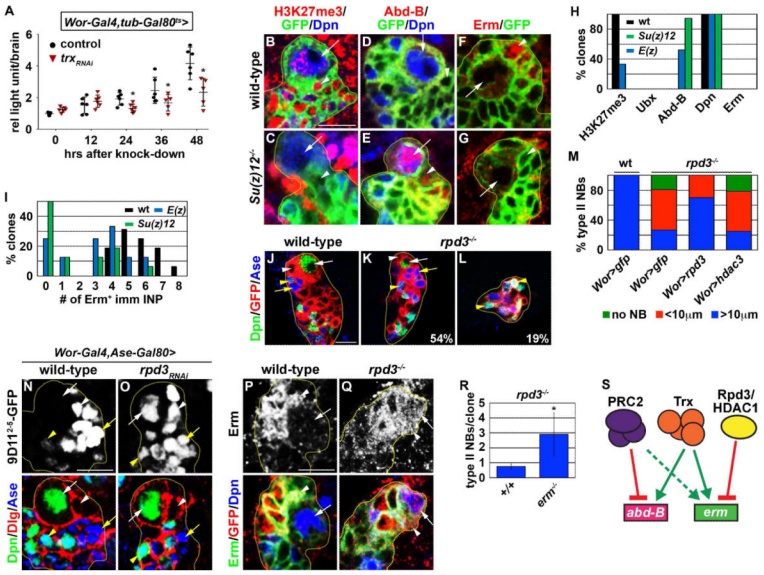

Figure 2. Rpd3-dependent deacetylation maintains the 9D11$^{2-5}$ enhancer poised in the type II neuroblast

(A) Single brain luciferase assay showing the effect of knocking down *trx* function on the activity of *9D11$^{2-5}$-GFP* relative to the control in wild-type brains (N ≥ 6 brains/time-point). (B-G) Confocal images of H3K27me3, Abd-B or Erm staining in 72hr wild-type or *Su(z)12$^{-/-}$* clones (outlined in yellow). (H) The percentage of wild-type, *E(z)$^{-/-}$* or *Su(z)12$^{-/-}$* type II neuroblasts that are positive for H3K27me3, Ubx, Abd-B, Dpn or Erm (N ≥ 10 clones/genotype). (I) The percentage of wild-type, *E(z)$^{-/-}$* or *Su(z)12$^{-/-}$* type II neuroblast clones that contain 0-8 Erm^{+} immature INPs. (J-L) Confocal images showing the effect of removing *rpd3* function on type II neuroblasts. (M) The percentage of *rpd3$^{-/-}$* type II neuroblasts that display the indicated phenotypes following over-expression of the indicated transgene for 72 hours (N ≥ 15 clones/genotype). (N-O) The effect of knocking down *rpd3* function on the expression of *9D11$^{2-5}$-GFP* in type II neuroblasts. (P-Q) The effect of removing *rpd3* function on endogenous Erm expression in type II neuroblasts. (R) The average number of neuroblasts in *rpd3$^{-/-}$* type II neuroblast clones in wild-type or *erm$^{-/-}$* brains (N = 5 brains each). (S) Schematic illustration of the regulation of *abd-B* and *erm* in wild-type type II neuroblasts. Solid red line with bar: repression, solid green line with arrow: direct role in activation, dotted green line with arrow: potential role in activation.

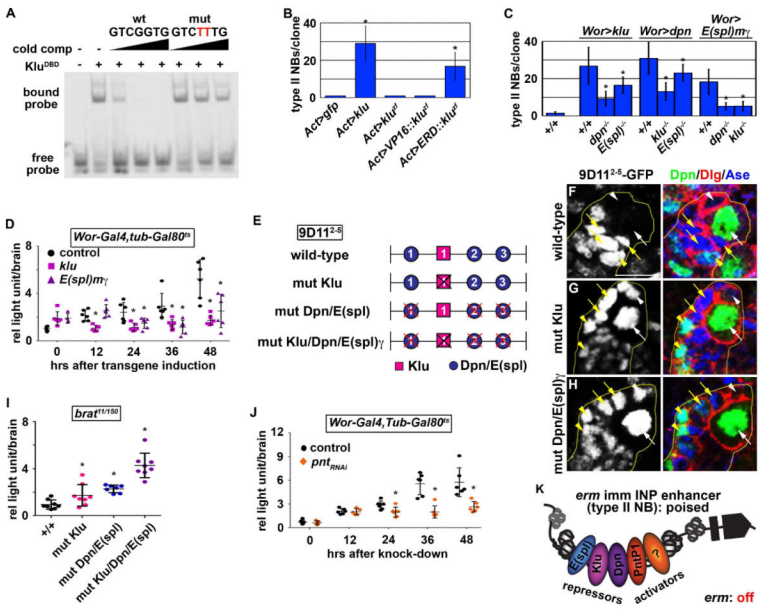

Figure 3. Dpn, E(spl)mγ, Klu and PntP1 directly bind and regulate the 9D11$^{2-5}$ enhancer activity

(A) Electromobility shift assay showing the interaction of the DNA-binding domain of Klu (Klu^{DBD}) with a putative Klu-binding site in the 9D11$^{2-5}$ enhancer. A wild-type and a mutant unlabeled probe serve as competitors to the wild-type labeled probe. (B) The average number of supernumerary neuroblasts in wild-type type II neuroblast clones over-expressing Klu, Klu^{zf}, VP16::Klu^{zf} or ERD::Klu^{zf} (N ≥ 10 clones/genotype). (C) The average number of supernumerary neuroblasts induced by over-expressing Klu, Dpn or E(spl)mγ in the type II neuroblast clones of the indicated genotypes (N ≥ 10 clones/genotype). (D) Single brain luciferase assay showing the effect of overexpressing Klu or E(spl)mγ on the activity of *9D11$^{2-5}$-GFP* relative to the control in wild-type brains (N ≥ 6 brains/time-point). (E) Schematic illustration of reporters containing wild-type or mutant binding sites on the 9D11$^{2-5}$ enhancer. (F-H) The expression pattern of wild-type or mutant *9D11$^{2-5}$-GFP* in the type II neuroblast lineage. (I) Single brain luciferase assay showing the activity of wild-type or mutant *9D11$^{2-5}$-GFP* in *brat* null brains (N ≥ 6 brains/time-point). (J) Single brain luciferase assay showing the effect of knocking down *pnt* function on the activity of *9D11$^{2-5}$-GFP* relative to the control in wild-type brains (N ≥ 6 brains/time-point). (K) A summary of transcription factors bound to the 9D11$^{2-5}$ enhancer in the type II neuroblast.

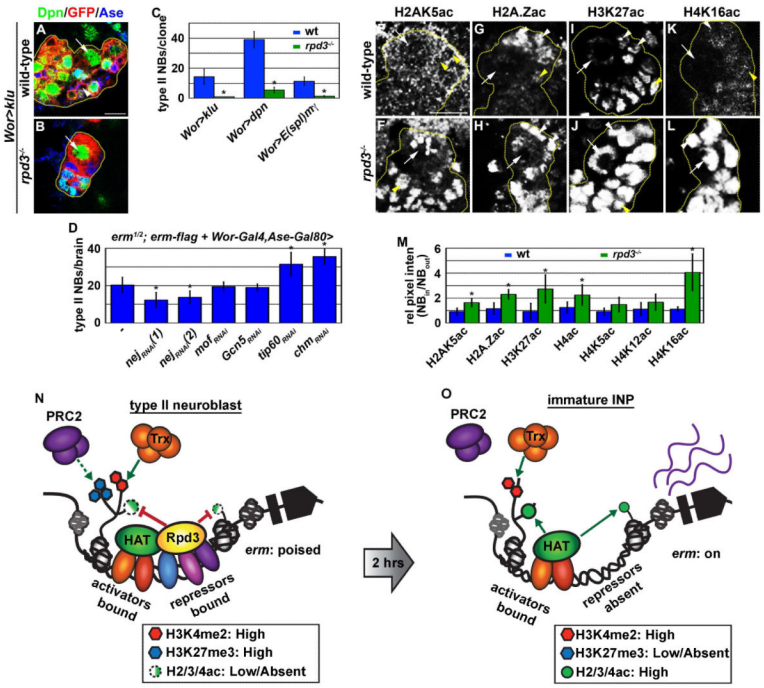

Figure 4. Dpn, E(spl)mγ and Klu function through Rpd3 to maintain *erm* in a poised state in type II neuroblasts by antagonizing the acetylation of multiple histones

(A-B) wild-type or *rpd3*$^{-/-}$ type II neuroblast clones overexpressing Klu. (C) The average number of supernumerary neuroblasts in wild-type or *rpd3*$^{-/-}$ type II neuroblast clones overexpressing Klu, Dpn or E(spl)mγ (N ≥ 10 clones/genotype). (D) The average number of supernumerary neuroblasts in *erm* hypomorphic mutant brains where the indicated HATs are knocked down by RNAi throughout type II neuroblast lineages (N ≥ 10 clones/genotype). (E-L) Confocal images showing the effect of *rpd3* mutation on the acetylation of the indicated residue(s) on histones in type II neuroblast clones. (M) Quantification of the pixel intensity approximating the level of acetylation on the indicated residue(s) of histones in type II neuroblast clones inside the wild-type or *rpd3*$^{-/-}$ clones relative to neuroblasts outside the clone. (N-O) Summary models showing how the *erm* immature INP enhancer is maintained in a poised state in type II neuroblasts and rapidly transitions to an activate state in immature INPs.

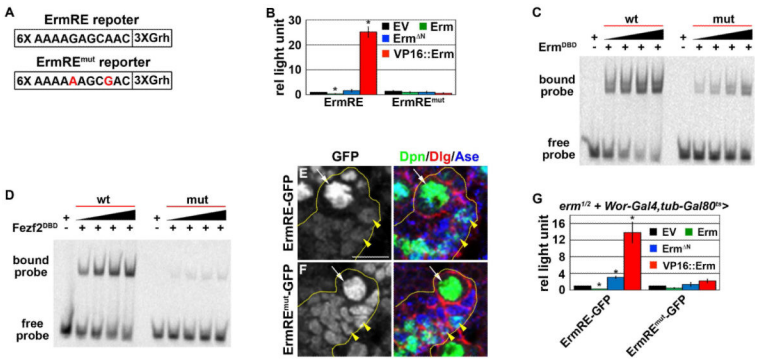

Figure 5. Identification of an Erm/Fezf consensus DNA-binding site

(A) Illustration of a wild-type (ErmRE) and a mutant (ErmRE^{mut}) Erm-response element used in *S2* cells and *in vivo* analyses. These reporters contain three Grainy head (Grh) binding sites to activate expression in larval neuroblast lineages. (B) Comparison of the relative expression levels of ErmRE-GFP::Luc(nls) and ErmRE^{mut}-GFP::Luc(nls) in response to the co-transfection with *erm, erm*$^{\Delta N}$ or *VP16::erm* in S2 cells (N ≥ 5 transfections/sample). EV: empty vector. (C-D) EMSA showing the interaction of the zinc-finger motif of Erm or Fezf2 with labeled probes bearing the sequence found in the ErmRE or ErmRE^{mut}. (E-F) Confocal images showing the expression of ErmRE-GFP::Luc(nls) or ErmRE^{mut}-GFP::Luc(nls) in the type II neuroblast lineage. (G) Single brain luciferase assay showing the effect of over-expressing *erm, erm*$^{\Delta N}$ or *VP16::erm* for 12 hours on the relative expression level of ErmRE-GFP::Luc(nls) or ErmRE^{mut}-GFP::Luc(nls) in *erm* null brains (N ≥ 3 samples/genotype).

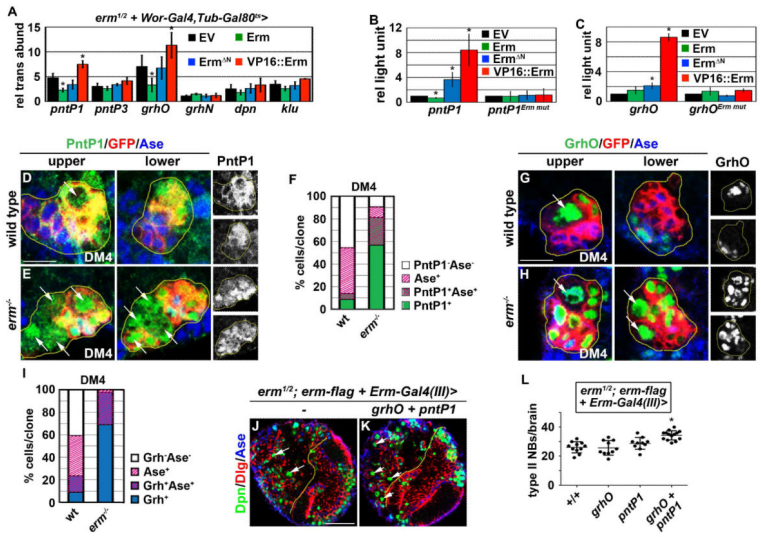

Figure 6. Erm restricts the developmental potential of INPs by repressing *pntP1* and *grhO* transcription

(A) qPCR analysis of the effect of over-expressing *erm*, *erm*$^{\Delta N}$ or *VP16::erm* for 12 hours on the abundance of *pntP1*, *pntP3*, *grhO*, *grhN*, *dpn* and *klu* transcripts in *erm* mutant brains relative to control brains (N ≥ 3 samples/genotype). (B) Comparison of the relative expression levels of reporters containing the *pntP1* promoter with wild-type (*pntP1*) or mutant (*pntP1*$^{Erm\ mut}$) Erm-binding sites in S2 cells co-transfected with *erm*, *erm*$^{\Delta N}$ or *VP16::erm* (N ≥ 3 transfections/sample). EV: empty vector. (C) Comparison of the relative expression levels of reporters containing the *grhO* promoter with wild-type (*grhO*) or mutant (*grhO*$^{Erm\ mut}$) Erm-binding sites in S2 cells co-transfected with *erm*, *erm*$^{\Delta N}$ or *VP16::erm* (N ≥ 3 transfections/sample). (D-E) Confocal images showing the effect of removing *erm* function on PntP1 expression in the DM4 type II neuroblast lineage clones. Upper/lower: the upper or lower confocal optical section of the z-series. (F) Quantification of the percentage of cells that are PntP1^{+}, Ase^{+} or PntP1^{+}Ase^{+} in the DM4 lineage clones of the indicated genotype (N ≥ 5 clones/genotype). (G-H) Confocal images showing the effect of removing *erm* function on GrhO expression in the DM4 type II neuroblast clones. Upper/lower: the upper or lower confocal optical section of the z-series. (I) Quantification of the percentage of cells that are GrhO^{+}, Ase^{+} or GrhO^{+}Ase^{+} in the DM4 lineage clones of the indicated genotype (N ≥ 5 clones/genotype). (J-K) Confocal images showing the effect of mis-expressing *pntP1* and *grhO* in Ase^{+} immature INPs and INPs in *erm* hypomorphic brains. Scale bar = 25 μm. (L) Quantification of the number of type II neuroblasts induced by mis-expression of *pntP1*, *grhO* or both in Ase^{+} immature INPs and INPs in *erm* hypomorphic brains.

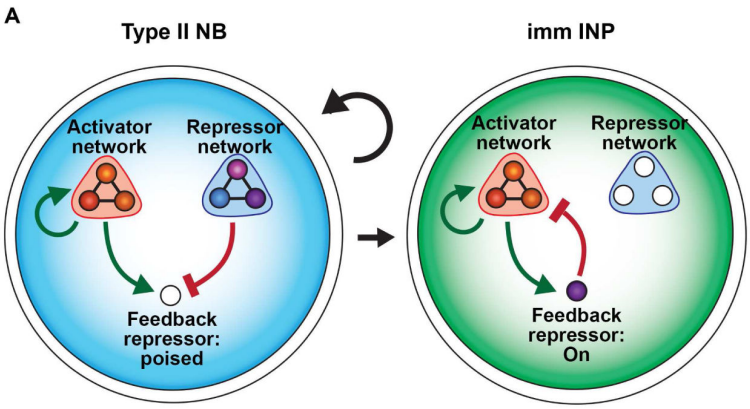

Figure 7. A poised feedback circuit balances continual self-renewal of type II neuroblasts with rapid restriction of the developmental potential in immature INPs

Summary model showing that balancing the activity of an activator network with a repressor network in the type II neuroblast maintains *erm* (feedback repressor) in an inactive but poised state to allow continual self-renewal. Following asymmetric division, downregulation of this repressor network allows for rapid activation of Erm expression in immature INPs where it represses components of the type II neuroblast activator network to stably restrict the developmental potential.